phys. stat. sol. (b) **240**, No. 3, 469–479 (2003) / **DOI** 10.1002/pssb.200303827

Many-body and overlayer effects on surface optical properties

F. Bechstedt[*, 1], **R. Del Sole**[2], **S. Glutsch**[1], **P. H. Hahn**[1], **O. Pulci**[2], and **W. G. Schmidt**[1]

[1] Institut für Festkörpertheorie und Theoretische Optik, Friedrich-Schiller-Universität, Max-Wien-Platz 1, 07743 Jena, Germany

[2] Istituto Nazionale per la Fisica della Materia, Dipartimento di Fisica dell' Universita' di Roma Tor Vergata, Via della Ricerca Scientifica 1, 00133 Roma, Italy

Received 30 May 2003, revised 4 August 2003, accepted 11 August 2003
Published online 25 November 2003

PACS 68.35.Bs, 71.15.Qe, 73.20.At, 78.68.+m

We demonstrate the potential of recently developed total-energy and electronic-structure methods for the calculation of the optical properties of real surfaces. The many-body effects are fully taken into account by a solution of the combined Dyson and Bethe-Salpeter equations. We show that an initial-value formulation of the polarization function allows an efficient numerical calculation of the optical susceptibility for large slabs consisting of many atoms. As examples we investigate GaP(001) and Si(001) surfaces covered by hydrogen. In the case of P-rich GaP(001)2 × 2–H surfaces the low-energy region of the reflectance anisotropy (RA) is dominated by electron–hole pair excitations in surface states. Surface-induced modifications of bulk excitons near the E_1 and E_2 transitions are responsible for the RA of the monohydride Si(001)2 × 1–H surface.

1 Introduction

Recent years have seen impressive methodological progress in the accurate numerical modeling of optical properties from first principles using the many-body perturbation theory (MBPT) [1]. It has become possible to compute single-particle electronic excitations in an accurate manner using Hedin's GW approximation (GWA) [2]. In addition, the Bethe-Salpeter equation (BSE) for electron–hole pair excitations can be solved in the framework of the same approximation, in order to account for excitonic and local-field (LF) contributions to the polarization function [3–5]. However, the large numerical effort required to solve the BSE has restricted such calculations to the interaction of relatively few electron–hole pairs. Therefore, the calculations of optical properties are usually limited to bulk semiconductors [6–10] or to semiconductor surfaces with strongly localized and energetically well separated states [11, 12]. There are only first trials to include more pair states in surface calculations, for instance to describe surface-modified bulk excitons [13].

At the same time, surface reflectance spectroscopies in the visible to near-UV spectral range have been successfully developed for monitoring surfaces during film growth by molecular beam epitaxy (MBE) and metalorganic vapor phase epitaxy (MOVPE) in real time. Special techniques such as reflectance anisotropy spectroscopy (RAS) are now frequently used not only for in situ diagnostic probes but also to obtain important information about the atomic structure of surfaces in various environments and with adsorbed species [14–16]. However, since this method gives only indirect information via the spectral variation of the RAS signal, a careful theoretical modeling is required and also possible to do [17, 18].

[*] Corresponding author: e-mail: bech@ifto.physik.uni-jena.de, Phone: +49 3641 947150, Fax: +49 3641 947152

Coverage by hydrogen gives stable overlayers of semiconductor surfaces, which may represent important intermediate steps of growth using MOVPE, chemical beam epitaxy (CBE) or gas-phase MBE. This holds for (001) substrates of both III–V semiconductors and silicon. Examples are the phosphorous-rich 2×1 or $2 \times 1/2 \times 2$ reconstructions of InP(001) and GaP(001) surfaces [19–25] as well as the single-domain monohydride-terminated Si(001)2×1 surface [26]. In discussing spectroscopic results for such surfaces, the role of hydrogen is sometimes overlooked. The zig-zag chains which have been clearly resolved by scanning tunneling microscopy (STM) on P-rich InP(001)2×1 surfaces [19, 21] have been interpreted as a violation of the electron counting principle [18, 27]. Strong electron correlation effects have been suggested to explain the insulating character of the surface by opening of a Mott-Hubbard gap [19]. An extensive computational search for H-free 2×1 geometries found symmetric, rather than asymmetric P dimers to be energetically favored for both InP(001)2×1 and GaP(001)2×1 [28–30]. The presence of hydrogen gives a natural explanation of the experimental findings concerning the insulating behavior [22]. On the other hand, there are also indications that Si-terminated SiC(001) surfaces show the opposite behavior and become metallic in the presence of hydrogen [31, 32].

In this paper the progress in the calculation of surface optical properties is discussed with a focus on the RAS. This not only concerns the computation of the geometries, thermodynamic phases, and electronic structures but also the inclusion of many-body effects in the framework of the MBPT. We show that the reflectance anisotropy (RA) of complicated surfaces can now be calculated from first principles. Hydrogen-covered (001) surfaces of semiconductors are used as examples. In Section 2 the computational methods are described. We present a novel numerically efficient approach to solve the BSE for the polarization function on the time domain using an initial-value formulation. The surface examples, P-rich GaP(001)$2 \times 1/2 \times 2$–H and Si(001)2×1–H, are discussed in detail in Section 3. A brief summary concludes the paper in Section 4.

2 Computational methods

2.1 Modeling of surfaces

In order to calculate the surface optical spectra we proceed in three steps. First, the energetically favored surface phase is identified and the equilibrium geometry is determined. The required total-energy and electronic-structure calculations are based on the density functional theory (DFT) [33] and the local density approximation (LDA) [34]. The electron-ion interaction is described by nonlocal norm-conserving pseudopotentials [35]. Semicore states are taken into account by nonlinear core corrections to the exchange and correlation energy. A massively parallel, real-space finite-difference method [36] is used to deal with the large unit cells needed to describe the surfaces. A multigrid technique accelerates the convergence. The spacing of the finest grid used to represent the electronic wave functions and charge density is about 10% of a bulk bond length.

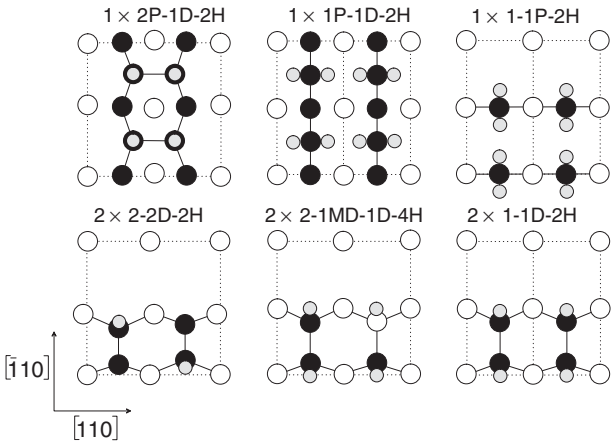

Fig. 1 The energetically most favorable GaP(001)–H surface structures (top view). Empty (filled, grey) circles represent Ga (P, H) atoms. A 2×2 area is shown.

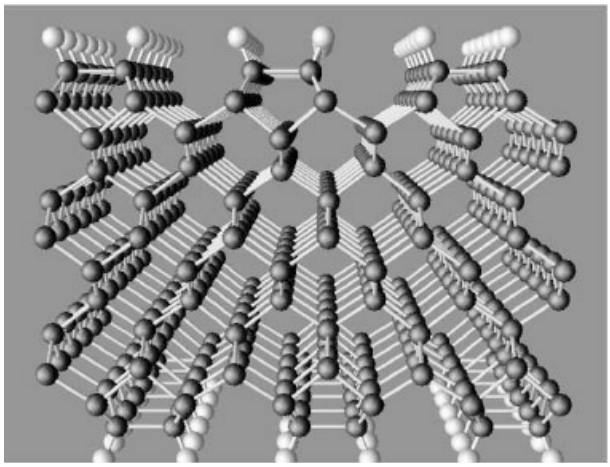

Fig. 2 Slab representing the monohydride phase of the Si(001)2×1–H surface.

The surfaces are modeled by periodic arrangements of supercells consisting of 16 (12) atomic layers in the GaP(001) [Si(001)] case. They are separated by vacuum regions large enough to decouple the surfaces. The computational details are like those in Ref. [37]. We use symmetric and asymmetric slabs to model the Si and GaP surface structures, respectively. In the latter case atoms in the lowest bilayer are kept frozen during the structural optimization, and the surface dangling bonds at the bottom layer are saturated by pseudohydrogen (hydrogen). We use a linear cutoff function to suppress the optical signal from the bottom layers in order to avoid spurious effects on the calculated spectra.

The possibility of hydrogen adsorption on gas-phase grown GaP(001) surfaces leads to a large number of conceivable models. We investigated more than 40 plausible structures [38], which differ with respect to their geometry, their Ga/ P ratio, and the number of adsorbed hydrogen atoms. The energetically favored hydrogen-induced surface reconstructions are shown in Fig. 1. The notation is such that a leading P indicates adsorption on top of a P-terminated substrate and a hyphen followed by P, D or MD denotes the adsorption of P atoms, P dimers or mixed Ga–P dimers, respectively. The number of hydrogen atoms per surface unit cell concludes the notation. In the case of Si(001)2 × 1 we only study a monohydride coverage, i.e., pairs of surface Si atoms form σ bonds and the second dangling bond of each Si atom is saturated by a H atom (cf. Fig. 2).

2.2 Reflectance anisotropy

The surface optical property of interest is the RA for normal incidence. For (001) surfaces the optical anisotropy between the light polarization directions $x \equiv [1\,\bar{1}0]$ and $y \equiv [110]$ is studied. The frequency-dependent RA can be obtained from slab calculations as [17, 18, 39]

$$\frac{\Delta R(\omega)}{R(\omega)} = \frac{8\pi\omega}{c}\,\mathrm{Im}\,\frac{\alpha_{xx}(\omega)-\alpha_{yy}(\omega)}{\varepsilon_b(\omega)-1}, \tag{1}$$

where $\alpha_{jj}(\omega)$ $(j = x;\ y)$ are the diagonal components of the half-slab polarizability tensor, and $\varepsilon_b(\omega) = 1 + 4\pi\alpha_b(\omega)$ is the corresponding bulk dielectric function.

We take advantage of the repeated-slab approximation. The Bloch picture is valid with wave vectors $\boldsymbol{k}$ from the surface Brillouin zone (BZ) and band indices v as good quantum numbers. Within the LDA to exchange and correlation the single-particle Kohn–Sham (KS) equation yields eigenfunctions $|v\boldsymbol{k}\rangle$ (or $\psi_{v\boldsymbol{k}}(\boldsymbol{x}) = \langle \boldsymbol{x} \mid v\boldsymbol{k}\rangle$) and eigenvalues $\varepsilon_v(\boldsymbol{k})$. The polarizability is related to the polarization function P. Within the Bloch picture one has [5, 18, 40]

$$\alpha_{jj}(\omega) = -\frac{2e^2\hbar^2}{V}\sum_{c,v,\boldsymbol{k}}\sum_{c',v'\boldsymbol{k}'}\{M^{j}_{cv}(\boldsymbol{k})\,M^{j*}_{c'v'}(\boldsymbol{k})\,P(cv\boldsymbol{k}, c'v'\boldsymbol{k}';\omega) + \text{c.c. and } \omega \leftrightarrow -\omega\} \tag{2}$$

with matrix elements of the velocity operator v

$$M_{cv}^{j}(\boldsymbol{k}) = \frac{\langle c\boldsymbol{k}|\, v_j \,|v\boldsymbol{k}\rangle}{\varepsilon_c(\boldsymbol{k}) - \varepsilon_v(\boldsymbol{k})} \tag{3}$$

and V as the normalization volume. In (2) the sums run over pairs of electrons in empty conduction band states $|c\boldsymbol{k}\rangle$ and holes in occupied valence band states $|v\boldsymbol{k}\rangle$, which are virtually or physically excited by photons. The effect of the photon wave vector is neglected. The polarization function P obeys a BSE. Neglecting the coupling of resonant and antiresonant electron–hole pairs as well as the non-particle-conserving contributions to the electron–hole interaction, the BSE is of the form

$$\sum_{c'',v'',\boldsymbol{k}''} \left\{ H(cv\boldsymbol{k},\, c''v''\boldsymbol{k}'') - \hbar(\omega + i\gamma)\, \delta_{cc''}\delta_{vv''}\delta_{\boldsymbol{k}\boldsymbol{k}''} \right\} P(c''v''\boldsymbol{k}'',\, c'v'\boldsymbol{k}';\, \omega) = -\delta_{cc'}\delta_{vv'}\delta_{\boldsymbol{k}\boldsymbol{k}'} \tag{4}$$

with the effective electron–hole pair Hamiltonian $H(cv\boldsymbol{k};\, c'v'\boldsymbol{k}')$ and a small damping γ of the pair excitations. The Hamiltonian of pairs of excited electrons and holes, more precisely, of quasielectrons and quasiholes, is given by [3, 5, 18, 40]

$$H(cv\boldsymbol{k}, c'v'\boldsymbol{k}') = [\varepsilon_c^{QP}(\boldsymbol{k}) - \varepsilon_v^{QP}(\boldsymbol{k})]\, \delta_{cc'}\delta_{vv'}\delta_{\boldsymbol{k}\boldsymbol{k}'} + W(cv\boldsymbol{k},\, c'v',\, \boldsymbol{k}') + \overline{v}(cv\boldsymbol{k},\, c',\, v',\, \boldsymbol{k}') \tag{5}$$

with the matrix elements

$$W(cv\boldsymbol{k},\, c'\, v'\, \boldsymbol{k}') = -\int d^3\boldsymbol{x} \int d^3\boldsymbol{x}'\, \psi_{c\boldsymbol{k}}^{*}(\boldsymbol{x})\;\; \psi_{c'\boldsymbol{k}'}(\boldsymbol{x})\, W(\boldsymbol{x},\, \boldsymbol{x}')\, \psi_{v\boldsymbol{k}}(\boldsymbol{x}')\, \psi_{v'\boldsymbol{k}'}^{*}(\boldsymbol{x}') \tag{6}$$

and

$$\overline{v}(cv\boldsymbol{k}, c'v'\boldsymbol{k}') = 2\int d^3\boldsymbol{x} \int d^3\boldsymbol{x}'\, \psi_{c\boldsymbol{k}}^{*}(\boldsymbol{x})\, \psi_{v\boldsymbol{k}}(\boldsymbol{x})\, \overline{v}(\boldsymbol{x} - \boldsymbol{x}')\, \psi_{c'\boldsymbol{k}'}(\boldsymbol{x}')\, \psi_{v'\boldsymbol{k}'}^{*}(\boldsymbol{x}') \tag{7}$$

of the (statically) screened Coulomb interaction $W(\boldsymbol{x};\, \boldsymbol{x}')$ [41] and a bare Coulomb interaction $\overline{v}(\boldsymbol{x} - \boldsymbol{x}')$. Only the short-range part of the latter is taken into account in agreement with the physical character of expression (7) as electron–hole exchange [4].

The screened contribution W (6) to the total electron–hole interaction includes the classical attraction of electron and hole as represented by the diagonal elements $c = c'$ and $v = v'$. It is responsible for the electron–hole binding in the Wannier-Mott exciton [42]. The other contributions represent the mixing of electron–hole pairs which is responsible for the redistribution of oscillator strength in optical spectra [6, 7, 40]. The electron–hole exchange term $\propto \overline{v}$ (7) [3, 43, 44] corresponds to the inclusion of LF effects [45, 46]. Indeed, in the bulk case it has been shown [44, 47] that the inclusion of $\overline{v}$ in the BSE (4) gives a polarization corresponding to the macroscopic dielectric susceptibility.

The excited electrons and holes also interact with the inhomogeneous electron gas of the system. This leads to an exchange-correlation self-energy Σ of the system beyond the exchange-correlation potential V_{XC} that is already used in the Kohn-Sham equation of the DFT-LDA. As a consequence, this renormalization gives rise to quasielectrons and quasiholes [1, 2, 18]. Assuming the same energetical ordering of the positions of the quasiparticle peaks and of the KS energies, the quasiparticle effects are included within first-order perturbation theory [48, 49]. The KS wave functions are not updated [50] and the DFT-LDA eigenvalues are corrected according to

$$\varepsilon_v^{QP}(\boldsymbol{k}) = \varepsilon_v(\boldsymbol{k}) + \Delta_v(\boldsymbol{k})\,, \tag{8}$$

$$\Delta_v(\boldsymbol{k}) = \langle v\boldsymbol{k}|\, \Sigma(\varepsilon_v^{QP}(\boldsymbol{k})) - V_{XC}\, |v\boldsymbol{k}\rangle\,. \tag{9}$$

The exchange-correlation self-energy operator Σ is taken within the GWA [2]. In the explicit calculations we introduce further approximations following the schemes by Hybertsen and Louie [51] and Bechstedt et al. [52] or Cappellini et al. [53]. For several semiconductor surfaces this approximate treatment of self-energy corrections (9) has been shown to result in excitation energies which are within 0.1 eV of the experimental values [13, 54].

2.3 Time-dependent formulation

Since the atomic geometry of a surface is known from the total-energy minimization procedure (cf. Sect. 2.1), the optical properties of a surface (2) can be calculated by solving the BSE (4) starting in the next step with a pair Hamiltonian (5) in DFT-LDA quality, $H(cv\boldsymbol{k}, c'v'\boldsymbol{k}') = [\varepsilon_c(\boldsymbol{k}) - \varepsilon_v(\boldsymbol{k})]\,\delta_{cc'}\delta_{vv'}\delta_{\boldsymbol{k}\boldsymbol{k}'}$ Then the many-body effects can be added by improvement of the Hamiltonian in the third step according to the inclusion of quasiparticle shifts (9) and electron–hole interactions W (6) and $\bar{v}$ (7). In principle, the last step (including W and $\bar{v}$) can be done by diagonalizing the Hamiltonian matrix (5) [6, 8–10, 55]. However, in contrast to surface optical features to which only a few band pairs contribute [11, 12, 55], the dimension of the matrices for the H-covered (001) surfaces becomes rather large. The number of pair states $cv\boldsymbol{k}$ is dominated by typically more than 100 $\boldsymbol{k}$ points needed to sample the surface BZ. At least two valence and conduction bands per atom have to be taken into account in order to cover the spectral region of several eV. Each slab contains about 24 atoms or more. This results in a dimension of the exciton Hamiltonian of about $N = 10^5 \ldots 10^6$. Even with powerful supercomputers, the diagonalization of matrices of this dimension, which scales as $O(N^3)$, is prohibitively slow.

Therefore, we follow an earlier idea by Glutsch et al. [56] to calculate the polarizability from the time evolution of a vector $|\Psi(t)\rangle$ with N elements, which are defined as

$$\sum_{c',v',\boldsymbol{k}'} M^j_{c'v'}(\boldsymbol{k}')\, P(cv\boldsymbol{k}, c'v'\boldsymbol{k}'; \omega) = \frac{i}{\hbar}\int_0^\infty \mathrm{d}t\, \mathrm{e}^{i(\omega+i\gamma)t}\Psi_{cv\boldsymbol{k}}(t)\,. \tag{10}$$

The evolution of the elements of $|\Psi(t)\rangle$ are driven by the pair Hamiltonian (5)

$$\sum_{c',v',\boldsymbol{k}'} H(cv\boldsymbol{k}, c'v'\boldsymbol{k}')\,\Psi_{c'v'\boldsymbol{k}'}(t) = i\hbar\frac{\partial}{\partial t}\Psi_{cv\boldsymbol{k}}(t) \tag{11}$$

with their initial values

$$\Psi_{cv\boldsymbol{k}}(0) = M^j_{cv}(\boldsymbol{k})\,. \tag{12}$$

We solve the initial-value problem by the central difference method [40, 57]. The upper limit of the Fourier integral in (10) can be truncated due to the exponential $\exp(-\gamma t)$. The number of time steps, i.e., the matrix-vector multiplications, is nearly independent of the dimension of the system. The operation count for this method scales thus quadratically with the rank of the pair Hamiltonian, N, and is therefore particularly suitable for complex systems such as surfaces. The time-dependent polarization function $\alpha_b(t) \propto \mathrm{Im}\,\langle M^j\,|\Psi(t)\rangle$ resulting for bulk silicon is plotted in Fig. 3. The CPU time savings resulting from using the novel time-dependent method versus the direct diagonalization of the Hamiltonian is demonstrated in Fig. 4.

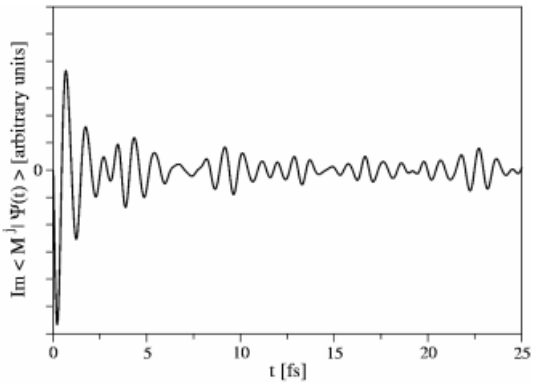

Fig. 3 Time-dependent polarization $\mathrm{Im}\langle M^j\,|\Psi(t)\rangle$ calculated for bulk Si [57].

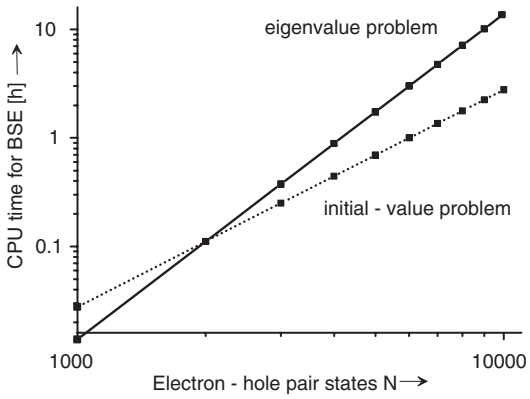

Fig. 4 CPU time needed to solve the BSE for bulk Si using the direct diagonalization of H (5) (eigenvalue problem) and the time-dependent formulation (11) (initial-value formulation) on a single Pentium PC.

3 Electronic structure and reflectance anisotropy

3.1 Hydrogen-covered P-rich GaP(001)2 × 1/2 × 2 surface: Surface-state transitions

Due to the varying surface stoichiometry, the thermodynamic grandcanonical potential Ω has to be studied in dependence on the chemical potentials μ of the surface constituents in order to determine the surface ground state for given preparation conditions. We focus our attention to the range of intermediate to slightly more P-rich preparation conditions for the substrate. The hydrogen chemical potential is fixed such as to describe MOVPE growth conditions. Then the 2 × 2–2D–2H structure (Fig. 1) represents the most favorable surface. It represents a periodic arrangement of oppositely buckled P dimers with buckling amplitude of 0.32 Å on top of a cation-terminated substrate. One H atom is bonded to the "down" atom of the P dimer.

The energetical arguments alone are only one indication that the 2 × 2–2D–2H structure corresponds to the surface observed experimentally. Its formation may be kinetically hindered. In order to clarify whether this structure indeed corresponds to the experimentally observed one, spectroscopic signatures have to be discussed. The surface bands calculated long high-symmetry lines of the 2 × 2 surface BZ are shown in Fig. 5. The surface band gap computed within DFT-LDA near Γ is slightly larger than 1 eV. The inclusion of quasiparticle effects results in its opening of about 0.6 eV [54]. Based on the calculated surface electronic structure (Fig. 5) we have also simulated STM images for bias voltages of ±3.5 V. The calculated filled-state image shows excellent agreement with experimental images measured for the P-terminated surface at sample bias 3.35V [25]. Zig-zag chains running along the [110] direction are observed. The bright spots forming the zig-zag pattern are mainly due to the lone-pair state V1 localized at the "up" atom of the P dimer (cf. Fig. 1). This state essentially forms the uppermost occupied surface band near *K*. This explains why only one P atom is seen in STM experiment. Arguments related to a violation of the electron counting rule or to the occurrence of strong electron correlation effects are not needed to explain the STM findings.

The electronic bands and wave functions in DFT-LDA quality represent the basis for the calculation of the surface optical properties according to expression (1). According to the experience with the RA spectra of many other polar (001) surfaces of III–V semiconductors [22, 23, 54, 58, 59], we assume that excitonic effects are negligible and replace the pair Hamiltonian (5) for a moment by the diagonal one, $H(cv\boldsymbol{k},c'v'\boldsymbol{k}') = [\varepsilon_c^{QP}(\boldsymbol{k}) - \varepsilon_v^{QP}(\boldsymbol{k})\,\delta_{cc'}\delta_{vv'}\delta_{\boldsymbol{k}\boldsymbol{k}'}$. In this way we were even able to explain the finestructure of the measured low-temperature RA spectra of InP(001)2 × 4 [59]. In the explicit computations done here we approximate the self-energy corrections (9) by using a rigid shift of 0.8 eV, which is the value we obtained for the GW corrections in GaP bulk [54, 60]. We use an energy broadening of $\hbar\gamma = 0.15$ eV in order to account for the lifetime broadening and the finite number of $\boldsymbol{k}$ points. A set equivalent to 1024 points in the full 1 × 1 surface BZ is used. The resulting RA spectrum is represented in Fig. 6 and compared with several experimental spectra [23–25].

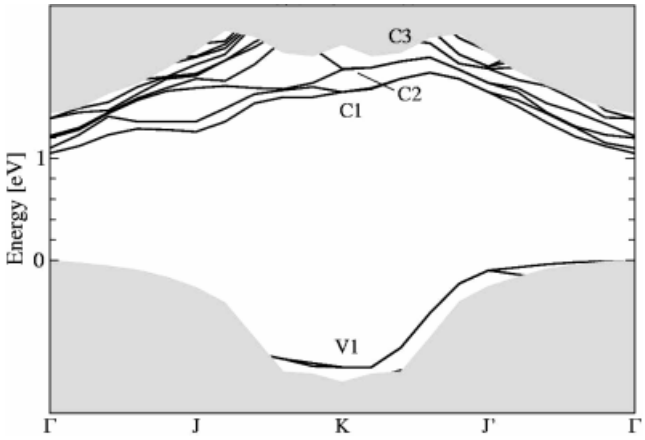

Fig. 5 (online colour at: www.interscience.wiley.com) Surface band structure (solid lines) of the GaP(001)2 × 2–2D–2H surface [38]. Grey regions indicate the projected bulk band structure.

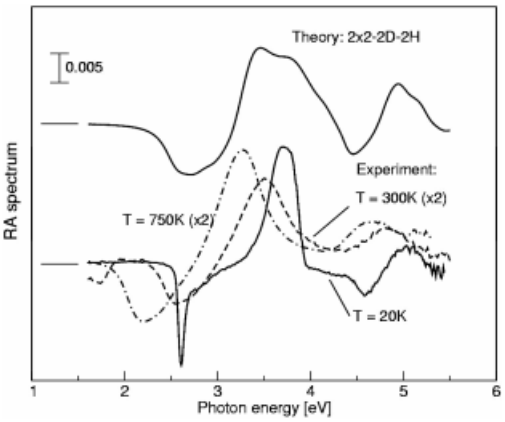

Fig. 6 Reflectance anisotropy spectrum of the GaP(001) 2×2–2D–2H structure [38]. The calculated one is compared with spectra for P-terminated GaP(001)$2 \times 1/2 \times 2$ surfaces measured at 20 K [25], 300 K [23], and 750 K [24].

The computed spectrum in Fig. 6 exhibits two significant negative and positive features. The broad minimum at around 2.5–2.9 eV is a clear fingerpoint of the H- and P-dimer-covered GaP(001) surface. This is clearly demonstrated in Fig. 7. For the low-energy range this figure indicates strong contributions of optical transitions from the uppermost occupied lone-pair states V1 which are localized at the "up" atom in each of the P dimers. The final states of the optical transitions are the lowest surface conduction band states C1, C2, and C3. They include strong contributions of σ^* antibonding states of the P dimers. However, in addition contributions from deformed Ga–P backbond states localized in the first bulklike Ga–P bilayer appear, in particular for C2 and C3. Taking into account the spectral broadening the position of this negative RA feature agrees reasonably with the corresponding negative peaks measured for room temperature [23] or low temperature [25]. This is valid in particular considering an overestimation of the quasiparticle shift of the surface-state transitions of about 0.2 eV. A detailed study of the quasiparticle effects for GaP(001)2×4 found the shift to be nonuniform: It amounts to about 0.6 eV for the surface-state-related features and 0.8–1.0 eV for features near the bulk critical points E_1 and E_2 [54], somewhat in contrast to the assumed rigid shift of 0.8 eV. The measured high-temperature phase [24] is probably remarkably disturbed with respect to the ideal 2×2–2D–2H structure. The narrowness of the negative peak at 2.6 eV in the measured low-temperature spectrum of Fig. 6 [25] may be interpreted as an indication for strong excitonic effects below the bulk absorption edge E_0.

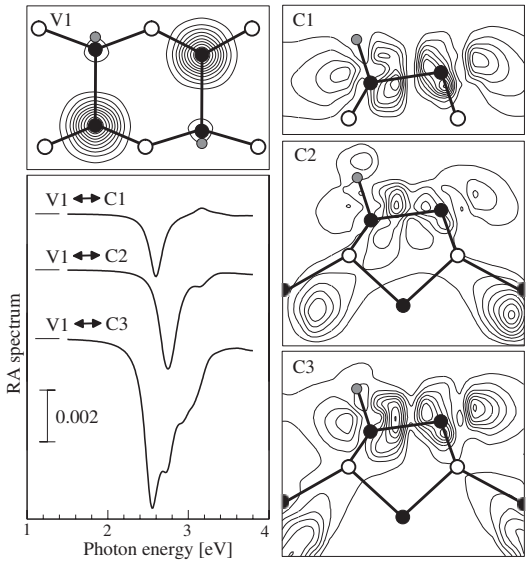

Fig. 7 Calculated RA contributions of optical transitions between certain surface bands as indicated in Fig. 5. The orbital character of the corresponding states at the K point of the surface BZ is shown (V1: top view, C1–C3: side views).

The RA in the high-energy region is dominated by surface-modified electronic transitions near the bulk critical-point (CP) energies E_1 = 3.8 eV, E_0' = 4.8 eV, and E_2 = 5.2 eV [61]. The lowest CP transitions with energies E_0 = 2.9 eV cannot really be identified in the RA spectra. The rigid hift of 0.8 eV guarantees that the theoretical (quasiparticle) values E_0 = 2.9 eV and E_0' = 4.8 eV approach the experimental ones. The two positive RA features around 3.4–3.8 eV and 4.8–5.2 eV are likely to be related to anisotropically deformed bulk Bloch states in the surface region. One may speculate that the sign of the negative RA feature around 4.5 eV indicates an anisotropy due to P dimer states.

3.2 Monohydride Si(001)2 × 1 surface: Surface-modified bulk excitons

The saturation of one dangling bond per surface Si dimer atom by a hydrogen atom (Fig. 2) generates symmetric dimers (more strictly speaking, σ-bonded pairs of Si atoms) with a bond length d_{dim} = 2.38 Å and a Si–H bond length of 1.48 Å. The vanishing tilting is accompanied by a small inward relaxation of the first atomic layer. As a consequence of the H adsorption the π and π^* bands (more strictly, D_{up} and D_{down} bands [18]) are removed from the fundamental gap. This passivation behavior is clearly demonstrated in Fig. 8. No surface bound states appear. Only surface resonance states can be observed. Occupied surface resonance bands are visible near the K point about 2 eV below the valence-band maximum. There are also indications for these surface bands along the KJ' and KJ lines in the 2 × 1 surface BZ.

After fixing the atomic geometry and the calculation of the accompanying band structure in DFT-LDA quality, most interesting is the development of the optical RA spectrum (1) with the inclusion of the various many-particle effects according to four approximations of the two-particle Hamiltonian (5). They are the independent-particle approximation (i.e., DFT-LDA), the independent-quasiparticle approximation (i.e., DFT-LDA with inclusion of self-energy effects in GW approximation), the independent-quasiparticle approach with electron–hole exchange (i.e., local-field effects), and the approach of quasiparticles with the full Coulomb correlation (i.e., screened electron–hole attraction and electron-hole exchange) of the quasielectrons and quasiholes. The corresponding resulting spectra are represented in Fig. 9. They are compared with measured RA data [26]. The RA spectrum in DFT-LDA quality exhibits several structures. Most significant are a positive RA feature close to the E_1 and E_0' transitions near 3 eV (called also A') and a negative peak at about the E_2 transitions near 3.6 eV (called B'). The significance of these spectral structures is underlined after inclusion of quasiparticle effects (i.e., within GWA). Due to the state dependence of the quasiparticle shifts the two peaks are enhanced and shifted to energies of about 3.65 and 4.25 eV. The other spectral features widely disappear or occur as shoulders (e.g., the structure at about 4 eV). Only a negative peak near 3.3 eV remains. In any case the inclusion of self-energy corrections calculated within the GW approximation (9) gives rise to a greater optical anisotropy than the less sophisticated DFT-LDA calculations. The model of a rigid quasiparticle shift for all optical transitions does not work for the Si(001)2 × 1–H surface.

The influence of LF effects (or equivalently electron–hole exchange) in Fig. 9 is rather weak. There is no significant energy shift or redistribution of oscillator strength. We made this observation already for

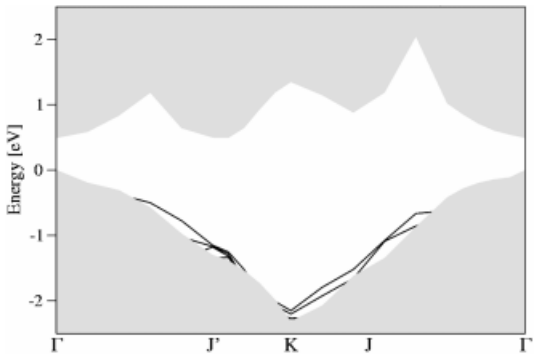

Fig. 8 Band structure of the Si(001)2 × 1–H surface in DFT-LDA quality. Grey regions indicate the projected bulk band structure.

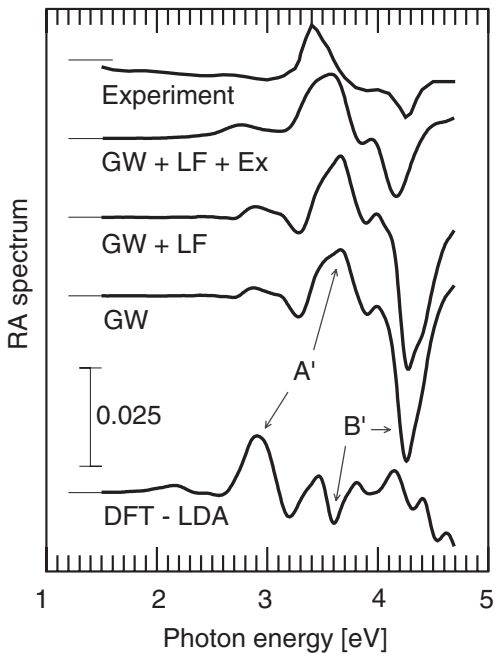

Fig. 9 RA spectrum calculated in different approximations with respect to the many-body effects for the monohydride Si(001)2 × 1–H surface [57]: within DFT-LDA (i.e., using KS eigenvalues $\varepsilon_v(\boldsymbol{k})$; in the GW approximation (i.e., shifted by quasiparticle shifts (9)); in the GWA with LF effects (i.e., $\overline{v}$ (7) is included in the Hamiltonian (5)), and in the GWA with LF effects and screened electron–hole attraction (i.e., the interactions $\overline{v}$ (7) and W (6) are fully included in the Hamiltonian (5)). The computed spectra are compared with measured data (i.e., experiment) [26].

the RA of the Si(110)1 × 1-H surface [13]. This finding somewhat contradicts the common believe that LF effects due to the presence of the surface should be important for the correct description of the surface RA [62–64]. Much more important are excitonic effects. The negative peak near 3.3 eV almost vanishes and oscillator strength is redistributed from the E_2 to the E_1/E_0' energy region. The later effect has been also observed for bulk Si [6, 57] and the Si(110)1 × 1–H surface [13]. It is mainly due to the coupling of electron–hole pairs (more strictly, quasielectron-quasihole pairs) from different energy regions by the screened Coulomb interaction W (6). In addition this effect also shifts the peaks towards smaller photon energies by about 0.1 eV.

The main contributions to the two resulting peaks A' and B' near photon energies of about 3.5 eV and 4.2 eV follow from the difference of the imaginary part of the two slab polarizabilities (2) for light polarizations $j = x$ and $j = y$. The difference effect is reduced by the factor $\mathrm{Re}\{1/[\varepsilon_b(\omega) - 1]\}$ which is of the order of 10. This is clearly demonstrated in Fig. 10. Interestingly the two polarizabilities for $j = x$ and y only show one pronounced peak with a maximum near E_2. A peak or a structure near the E_1 transition is widely missing for both polarization directions. This is in clear contrast to the findings for the Si(110)1 × 1–H surface [13].

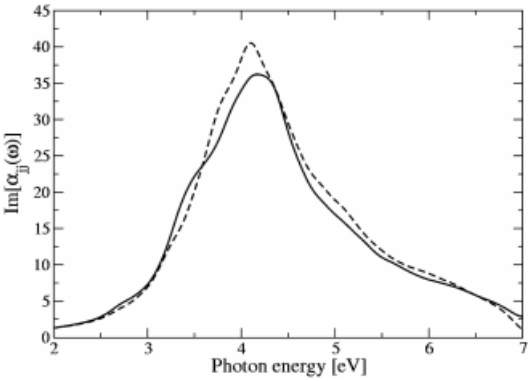

Fig. 10 Imaginary part of the slab polarizability (2) of Si(001)2 × 1–H for two directions of the light polarizations. Solid line: $j \equiv x$, dashed line: $j \equiv y$ The calculations were performed including quasiparticle, LF and electron–hole attraction effects.

The final RA spectra in Fig. 9 with all the many-particle effects (curve GW + LF + Ex) brings the lineshape and the peak positions of the theoretical RA close to those of the measured spectrum which is characterized by positive and negative peaks around 3.4 (A') and 4.3 eV (B') [26]. The low-energy peak around 3.4 eV has also been observed in an earlier study [65], in which a wet process has been used to prepare the surface. As a consequence of the relationship of the two peaks to the CPs E_1, E_0', and E_2 the surface optical anisotropy is explained as modulation of the bulk dielectric function.

4 Summary

We have demonstrated the recent progress in the theoretical description of surface optical properties. The reflectance anisotropy is considered as model property and the hydrogen-covered P-rich GaP(001)2 × 2 and Si(001)2 × 1 surfaces as prototypical systems. We have shown that the theory is able to predict optical properties also for surfaces relevant in gas-phase or chemical-beam epitaxies. The precision of the calculations allows not only for the identification of specific surface structures or surface-induced spectral features for the optimized geometry of a certain overlayer but also for the determination of lineshapes and peak positions with an accuracy of about 0.1–0.2 eV. Contributions of optical transitions between surface states and of surface-modified bulk excitons can be described and shown to influence the reflectance anisotropy spectra of (001) surfaces covered by a hydrogen overlayer. The stepwise inclusion of many-particle effects in the calculation leads to a considerable and systematic improvement of the agreement with the experiment. In contrast, the spectral modifications due to local-field effects are negligible for these surfaces. The applicability of the many-body perturbation theory to large systems has been explicitly demonstrated by calculating the optical anisotropy of the monohydride Si(001)2 × 1 surface. The progress has been made possible by the availability of powerful, massively parallel computers and the development of algorithms which allow for the treatment of many electron–hole-pair states in an effcient, yet accurate manner.

Acknowledgement Grants of computer time from the Leibniz-Rechenzentrum München, the Höchstleistungsrechenzentrum Stuttgart, the John von Neumann-Institut, and the INFM under 'Iniziativa Transversale Calcolo Parallelo' at CINECA are gratefully acknowledged. This work has been supported by INFM-PRA 1MESS, MIUR COFIN 2002, INFM-PAIS- Celex and by the EU through the NANOPHASE Research Training Network (Contract No. HPRN-CT-2000-00167). P. H. H. has been supported by a Marie Curie fellowship of the EU programme MAPS under the contract number HPMT-CT-2001-00242.

References

[1] G. Onida, L. Reining, and A. Rubio, Rev. Mod. Phys. **74**, 601 (2002).
[2] L. Hedin, Phys. Rev. 139, A796 (1965).
L. Hedin and S. Lundqvist, Solid State Phys. **23**, 1 (1969).
[3] L. J. Sham and T. M. Rice, Phys. Rev. **144**, 708 (1966).
[4] W. Hanke and L. J. Sham, Phys. Rev. B **21**, 4656 (1980).
[5] G. Strinati, Riv. Nuovo Cimento **11**, 1 (1988).
[6] S. Albrecht, L. Reining, R. Del Sole, and G. Onida, Phys. Rev. Lett. **80**, 4510 (1998).
[7] L. X. Benedict, E. L. Shirley, and R. B. Bohn, Phys. Rev. Lett. **80**, 4514 (1998); Phys. Rev. B **57**, R9385 (1998).
[8] M. Rohlfing and S. G. Louie, Phys. Rev. Lett. **81**, 2312 (1998).
[9] B. Arnaud and M. Alouani, Phys. Rev. B **63**, 085208 (2001).
[10] P. Puschnig and C. Ambrosch-Draxl, Phys. Rev. B **66**, 165105 (2002).
[11] M. Rohlfing and S. G. Louie, Phys. Rev. Lett. **83**, 856 (1999).
[12] M. Rohlfing, M. Palummo, G. Onida, and R. Del Sole, Phys. Rev. Lett. **85**, 5440 (2000).
[13] P. H. Hahn, W. G. Schmidt, and F. Bechstedt, Phys. Rev. Lett. **88**, 016402 (2002).
[14] J. F. McGilp, Prog. Surf. Sci. **49**, 1 (1995).
[15] W. Richter and J. F. Zettler, Appl. Surf. Sci. **100/101**, 465 (1996).
[16] D. E. Aspnes, Solid State Commun. **101**, 85 (1997).
[17] R. Del Sole, in: Photonic Probes of Surfaces, edited by P. Halevi (Elsevier Sci. Publ. Co., Amsterdam, 1995).

[18] F. Bechstedt, Principles of Surface Physics (Springer, Berlin, 2003).
[19] L. Li, B.-K. Han, Q. Fu, and R. F. Hicks, Phys. Rev. Lett. **82**, 1879 (1999).
[20] L. Li, B.-K. Han, D. Law, C. H. Li, Q. Fu, and R. F. Hicks, Appl. Phys. Lett. **75**, 683 (1999).
[21] P. Vogt, Th. Hannappel, S. Visbeck, K. Knorr, N. Esser, and W. Richter, Phys. Rev. B **60**, R5117 (1989).
[22] W. G. Schmidt, P. H. Hahn, F. Bechstedt, N. Esser, P. Vogt, A. Wange, and W. Richter, Phys. Rev. Lett. **90**, 126101 (2003).
[23] A. M. Frisch, W. G. Schmidt, J. Bernholc, M. Pristovsek, N. Esser, and W. Richter, Phys. Rev. B **60**, 2488 (1999).
[24] M. Zorn, B. Junno, T. Trepk, S. Bose, L. Samuelson, J. T. Zettler, and W. Richter, Phys. Rev. B **60**, 11557 (1999).
[25] L. Töben, Th. Hannappel, K. Mölker, H.-J. Crawack, C. Pettenkofer, and F. Willig, Surf. Sci. **494**, L755 (2001).
[26] R. Shioda and J. van der Weide, Appl. Surf. Sci. **130–132**, 266 (1998).
[27] M. D. Pashley, Phys. Rev. B **40**, 10481 (1989).
[28] O. Pulci, K. Lüdge, W. G. Schmidt, and F. Bechstedt, Surf. Sci. **464**, 272 (2000).
[29] O. Pulci, W. G. Schmidt, and F. Bechstedt, phys. stat. sol. (b) **184**, 105 (2001).
[30] O. Pulci, K. Lüdge, P. Vogt, N. Esser, W. G. Schmidt, W. Richter, and F. Bechstedt, Comput. Mater. Sci. **22**, 32 (2001).
[31] V. Derycke, P. G. Soukiassian, F. Amy, Y. J. Chabal, M. D. D'Angelo, H. B. Enriquez, and M. G. Silly, Nature Mater. **2**, 253 (2003).
[32] V. M. Bermudez, Nature Mater. **2**, 218 (2003).
[33] P. Hohenberg and W. Kohn, Phys. Rev. B **136**, 864 (1964).
[34] W. Kohn and L. J. Sham, Phys. Rev. A **140**, 1133 (1965).
[35] M. Fuchs and M. Scheffler, Comput. Phys. Commun. **119**, 67 (1999).
[36] E. L. Briggs, D. J. Sullivan, and J. Bernholc, Phys. Rev. B **54**, 14362 (1996).
[37] W. G. Schmidt, Appl. Phys. A **75**, 89 (2002).
[38] P. H. Hahn, W. G. Schmidt, F. Bechstedt, O. Pulci, and R. Del Sole, Phys. Rev. B **68**, 033311 (2003).
[39] F. Manghi, R. Del Sole, A. Selloni, and E. Molinari, Phys. Rev. B **41**, 9935 (1990).
[40] F. Bechstedt, W. G. Schmidt, and P. H. Hahn, phys. stat. sol. (a) **188**, 1383 (2001).
[41] F. Bechstedt, K. Tenelsen, B. Adolph, and R. Del Sole, Phys. Rev. Lett. **78**, 1528 (1997).
[42] G. D. Mahan, Many-Particle Physics (Plenum Press, New York, 1990).
[43] W. Hanke and L. J. Sham, Phys. Rev. B **12**, 4501 (1975).
[44] R. Del Sole and E. Fiorino, Phys. Rev. B **29**, 4631 (1984).
[45] S. Adler, Phys. Rev. **126**, 413 (1962).
[46] N. Wiser, Phys. Rev. **129**, 62 (1963).
[47] P. Hahn, Diploma thesis, Friedrich-Schiller-Universität Jena 2001.
[48] M. S. Hybertsen and S. G. Louie, Phys. Rev. **34**, 5390 (1986).
[49] F. Bechstedt, Festkörperprobleme/Adv. Solid State Phys. **32**, 161 (1992).
[50] O. Pulci, F. Bechstedt, G. Onida, R. Del Sole, and L. Reining, Phys. Rev. B **60**, 16758 (1999).
[51] M. S. Hybertsen and S. G. Louie, Phys. Rev. B **37**, 2733 (1988).
[52] F. Bechstedt, R. Del Sole, G. Cappellini, and L. Reining, Solid State Commun. **84**, 765 (1992).
[53] G. Cappellini, R. Del Sole, L. Reining, and F. Bechstedt, Phys. Rev. B **47**, 9892 (1993).
[54] W. G. Schmidt, J. L. Fattebert, J. Bernholc, and F. Bechstedt, Surf. Rev. Lett. **6**, 1159 (1999).
[55] M. Rohlfing and S. G. Louie, Phys. Rev. B **62**, 4927 (2000).
[56] S. Glutsch, D. S. Chemla, and F. Bechstedt, Phys. Rev. B **54**, 11592 (1996).
[57] W. G. Schmidt, S. Glutsch, P. H. Hahn, and F. Bechstedt, Phys. Rev. B **67**, 085307 (2003).
[58] W. G. Schmidt, E. L. Briggs, J. Bernholc, and F. Bechstedt, Phys. Rev. B **59**, 2234 (1999).
[59] W. G. Schmidt, N. Esser, A. M. Frisch, P. Vogt, J. Bernholc, F. Bechstedt, M. Zorn, Th. Hannappel, S. Visbeck, and W. Richter, Phys. Rev. B **61**, R16335 (2000).
[60] O. Pulci, M. Palummo, V. Olevano, G. Onida, L. Reining, and R. Del Sole, phys. stat. sol. (a) **188**, 1261 (2001).
[61] S. Zollner, M. Garriga, J. Kirchner, J. Humlíček, M. Cardona, and G. Neuhold, Phys. Rev. B **48**, 7915 (1993).
[62] B. S. Mendoza and W. L. Mochán, Phys. Rev. B **53**, R10473 (1996).
[63] D. Herrendörfer and C. H. Patterson, Surf. Sci. **375**, 210 (1997).
[64] B. S. Mendoza, R. Del Sole, and A. I. Shkrebtii, Phys. Rev. B **57**, R12709 (1998).
[65] A. B. Müller, F. Reinhard, U. Resch, W. Richter, K. C. Rose, and U. Rossow, Thin Solid Films **233**, 19 (1993).